Recombination of the Hydrated Electron at High Temperature and Pressure in Hydrogenated Alkaline Water

Timothy W. Marin

Chemistry Department, Benedictine University, Lisle, Illinois 60532

Kenji Takahashi

Department of Chemistry and Chemical Engineering, Kanazawa University, Kanazawa 920-8667, Japan

Charles D. Jonah and Sergey D. Chemerisov

Chemistry Division, Argonne National Laboratory, Argonne, Illinois 60439

David M. Bartels*

Notre Dame Radiation Laboratory, Notre Dame, Indiana 46556

Received: June 13, 2007; In Final Form: August 8, 2007

Pulse radiolysis experiments were performed on hydrogenated, alkaline water at high temperatures and pressures to obtain rate constants for the reaction of hydrated electrons with hydrogen atoms ($H^\bullet + e^-_{aq} \rightarrow H_2 + OH^-$, reaction 1) and the bimolecular reaction of two hydrated electrons ($e^-_{aq} + e^-_{aq} \rightarrow H_2 + 2\ OH^-$, reaction 2). Values for the reaction 1 rate constant, k_1, were obtained from 100 − 325 °C, and those for the reaction 2 rate constant, k_2, were obtained from 100 − 250 °C, both in increments of 25 °C. Both k_1 and k_2 show non-Arrhenius behavior over the entire temperature range studied. k_1 shows a rapid increase with increasing temperature, where $k_1 = 9.3 \times 10^{10}$ M^{-1} s^{-1} at 100 °C and 1.2×10^{12} M^{-1} s^{-1} at 325 °C. This behavior is interpreted in terms of a long-range electron-transfer model, and we conclude that e^-_{aq} diffusion has a very high activation energy above 150 °C. The behavior of k_2 is similar to that previously reported, reaching a maximum value of 5.9×10^{10} M^{-1} s^{-1} at 150 °C in the presence of 1.5×10^{-3} *m* hydroxide. At higher temperatures, the value of k_2 decreases rapidly and above 250 °C is too small to measure reliably. We suggest that reaction 2 is a two-step reaction, where the first step is a proton transfer stimulated by the proximity of two hydrated electrons, followed immediately by reaction 1.

Introduction

For several years, we have been working to generate the rate constant and product yield data needed to accurately model radiation-induced chemistry in the primary heat transport systems of existing and proposed water-cooled nuclear reactors. To predict the effects of the radiation on the cooling system chemistry, it is necessary to understand the yields and kinetics of the radiolytic transients over a wide range of reactor operating temperatures. New results for several important reactions have recently been reported up to 350 °C and higher.[1−9] In our continuing study of high-temperature and -pressure water radiation chemistry by electron pulse radiolysis, we have reexamined two critical reactions involving the hydrated electron (e^-_{aq}), in the 100−325 °C temperature range, those being its reaction with hydrogen atoms ($H^\bullet$)

$$H^\bullet + e^-_{aq} \rightarrow H_2 + OH^- \qquad (1)$$

and the bimolecular recombination of two hydrated electrons

$$e^-_{aq} + e^-_{aq} \rightarrow H_2 + 2OH^- \qquad (2)$$

* Corresponding author. Tel.: (574) 631-5561; fax: (574) 631-6652; e-mail: bartels@hertz.rad.nd.edu.

In addition to their practical importance, both reactions are fascinating from the point of view of fundamental chemical physics.

The reaction 1 rate constant, k_1, was previously reported in three separate pulse radiolysis/transient absorption studies.[10−12] While data from all three studies are roughly in agreement, the data from Christensen et al. were acquired over the widest temperature range, 20−250 °C.[10] These results indicated Arrhenius behavior over the entire temperature range, with an activation energy of 14.0 kJ mol^{-1}, near that expected for a diffusion-limited reaction.

The reaction 2 rate constant, k_2, was investigated in numerous studies over several decades,[11,13−24] and again, Christensen et al. provide data over the widest range of temperatures, in this case 5−300 °C.[17] These experiments also probed the second-order decay at multiple hydroxide (OH^-) concentrations up to 10^{-1} M. In their study, k_2 was observed to show Arrhenius behavior up to 150 °C, with a diffusion-controlled activation energy of 23 kJ mol^{-1}. Between 150 and 250 °C, k_2 rapidly decreased but then remained nearly constant up to 300 °C. No notable pH effect was observed for pH > 10. At lower pH values, k_2 was observed to significantly increase. Unfortunately, silicate was present at high temperatures from the dissolution of the quartz sample cell used, making the interpretation of those results difficult.

10.1021/jp074581r CCC: $37.00
Published on Web 10/12/2007

In the current paper, we reinvestigate both reactions 1 and 2 through electron pulse radiolysis/transient absorption. Measurements were conducted from 100 − 325 °C using multiple OH^- concentrations and radiation doses at each temperature. We reconfirm the non-Arrhenius behavior of the reaction 2 rate constant and provide new rate constant values above 200 °C that are significantly lower than previous results. The reaction 1 rate constant is shown to exhibit non-Arrhenius behavior as well, with an activation energy that gradually increases between 100 and 325 °C. This increase is discussed in the context of a diffusion-limited electron-transfer (ET) mechanism, and it is inferred that relative diffusion of $H^\bullet$ and e^-_{aq} must greatly increase above 200 °C. A new mechanism for reaction 2 is proposed, which appears to be consistent with all data and recent simulation studies.

Experimental Procedures

Pulse radiolysis experiments were performed using 4−40 ns pulses from the Argonne Chemistry Division's 20 MeV electron linac to obtain the range of radiation doses required for these experiments. The high-temperature/-pressure sample cell, flow system, and basic experimental setup and characteristics have been described in previous publications.[1,2,5,6,25] Experimental temperature and pressure stabilities were ±0.2 °C and ±0.1 bar, respectively. Analyzing light from a pulsed 75 W xenon lamp (Photon Technology International) was selected using 40 nm bandwidth interference filters (Andover Corporation) with center wavelengths corresponding to the maximum absorption of e^-_{aq} at each temperature. The red shift and width of the e^-_{aq} spectrum at elevated temperature was the subject of a recent publication.[26] A germanium photodiode (GMP566, Germanium Power Devices, Inc.) was used for detection. The inherent biexponential transient response of the photodiode[27] was accounted for in the data fitting as a convolution with the e^-_{aq} absorption. Kinetics were measured from 100 to 325 °C in steps of 25 °C. Data could not be acquired at very high OH^- concentrations ($>3 \times 10^{-4}$ *m*) above 300 °C as significant corrosion occurred in the sample cell, altering the e^-_{aq} kinetics. Data also could not be acquired at temperatures higher than 325 °C in the presence of any added OH^-, as significant corrosion occurred.

In preparing samples, standardized 0.991 M potassium hydroxide (KOH) solutions (Aldrich, used as received) were diluted to the appropriate concentration in deionized water (18.2 MΩ cm, Barnstead Nanopure system). Alkaline water samples were kept under nitrogen or argon at all times to avoid contamination by carbonate ions arising from possible carbon dioxide absorption and were purged with argon gas for at least 30 min prior to collecting data. Pressurized, hydrogenated water samples were prepared in our laboratory-built gas−liquid saturator. Details of this device have been previously published.[5] Hydrogen concentrations ranged from 0.037 − 0.080 *m* for all experiments.

Individual control over the hydrogenated water and KOH solution flow rates was achieved with two separate HPLC pumps (Alltech 301). The hydrogen concentration was kept constant in the sample cell over the course of a day's experiments and ranged in value from 0.036 − 0.072 *m*, depending on the pressure in the cylinder supplying the hydrogen gas. Four or five different KOH solutions were typically used to give total OH^- concentrations of 1.00×10^{-2}, 4.00×10^{-3}, 1.50×10^{-3}, 3.00×10^{-4}, and 1.00×10^{-4} *m* in the sample cell, with solution concentrations considered reliable within 2%. Note that we make use of molal units in referring to solute concentrations for the majority of this text. Since the water density decreases with increasing temperature, molal solute concentrations are conserved, but molar concentrations decrease. For the purpose of fitting rate constants, the solute concentrations were converted to molar units using water densities calculated with the IAPWS-IF97 formulation for light water PVT relations.[28]

Water radiolysis is kinetically complex and may involve some 50 competing reactions.[29] One of the primary species formed in radiolysis is the hydrated electron. Because of its large extinction coefficient ($\epsilon_{max} = 18\,400$ M^{-1} cm^{-1} at room temperature[17]), it is convenient to monitor this species via transient absorption to follow the radiation-induced kinetics. In hydrogenated alkaline water and with small radiation doses, the transient absorption from e^-_{aq} can be approximated by just three dominant reactions

$$H_2 + OH^\bullet \rightarrow H^\bullet + H_2O \tag{3}$$

$$H^\bullet + OH^- \leftrightarrow e^-_{aq} + H_2O \tag{4}$$

$$e^-_{aq} + e^-_{aq} \leftrightarrow 2OH^- + H_2 \tag{2}$$

The overall reaction scheme has been previously discussed.[6] In essence, reactions 3 and 4 are fast, occurring in the pseudo-first-order limit, leaving only e^-_{aq} in solution to recombine via reaction 2. With higher doses of radiation, other second-order reactions become involved in the kinetics, the most important being reaction 1. Under our experimental conditions, reaction 1 is the only second-order reaction fast enough to compete with the rates of reactions 3 and 4. The temperature dependence of the reaction 3 and 4 rate constants has recently been reported.[5,6]

Under the given alkaline hydrogenated conditions, e^-_{aq} is known to have a long lifetime, as evidenced by an absorption that lasts for tens of microseconds. Consequently, any impurities present in the water (metal ions, organics, etc.) can scavenge the e^-_{aq} species and compete with its bimolecular recombination. Experimentally, we have found this to be a problem, even with the high-purity water used in sample preparation. Although our radiolysis experiments generally have made use of a flow-through system in the past, here it was advantageous to experiment with a static sample. The sample flow was stopped just prior to collecting data by closing an exit valve for the effluent. Using the HPLC pumps, the sample was allowed to accumulate and pressurize in the sample cell until a constant pressure of 250 bar was achieved. Thereafter, cleaning radiation pulses from the linac were applied to the sample to reduce all reducible impurities in the hydrogenated water. Over the course of this irradiation, one could spectroscopically witness the lifetime of e^-_{aq} gradually increasing as the impurities were reduced. Although the number of pulses needed to extend the e^-_{aq} lifetime varied depending on the day, sample contents, and condition of flow system (new vs used tubing, windows, etc.), typically 10−20 pulses were necessary for a fresh sample, with a dose of ~100 Gy each. A few cleaning pulses were also then applied to the sample just before actual data collection to ensure that impurities were not building up. Normally, the same sample was used for all the data collected at a single temperature and OH^- concentration, and the sample cell was flushed and refilled for a new OH^- concentration or a new temperature. At times when impurity buildup was becoming substantial, the sample cell was disassembled, cleaned, and placed overnight in an oven at 350 °C to help reestablish a more corrosion-resistant metal oxide surface.

Two entire data sets were acquired, one in a high-dose regime (~50−100 Gy) and one in a low-dose regime (~10−50 Gy), where the linac was tuned on a chosen day for the dose regime in which to operate. Within a dose regime, at least three different doses were applied for a given sample before refilling with a new solution having a different OH^- concentration or changing to a different temperature. Although the dose was not measured on every shot, the linac pulses were stable to within 5% or better over the course of a day. The relative dose in each experimental set was measured by integrating charge on a thick copper shutter inserted between the beam port and the sample cell.

Fitting Model

The data were fit using a differential equation model that incorporates all of the known recombination reactions as well as yields of water radiolysis species at high temperatures. This model has been previously described and is continuously updated to incorporate the latest water radiolysis product yield and rate constant data.[2,6] To be consistent with the chemical literature, the fitting program incorporates the changes in water density as a function of temperature and converts molal solute concentrations to molar units. Rate constants are thus displayed in molar units in our tables and Arrhenius plots, vide infra. A computer program was set up to fit the e^-_{aq} kinetics by fitting the reaction rate constants of choice, while keeping all other (known) parameters of the model fixed. A sensitivity analysis for all the radiolysis rate constants confirmed that for the radiation doses and OH^- concentrations used in these studies, only k_{1-4} need be examined in detail, as individual changes to other rate constants in the model negligibly affect the fitted k_1 and k_2 values. These other reactions do, however, affect the quality of the fit. The quality of the fit gives us confidence that we are indeed correctly describing the experimental system. The fits were simplified by fixing rate constants k_3 and k_4 based on previous studies.[5,6] Global fits to k_1 and k_2 were performed over all applied doses for a given temperature and OH^- concentration. Unfortunately, at the lower temperatures studied (100−175 °C), the value of k_1 exceeded that of k_2 by less than a factor of 10, and their rate coefficients were strongly correlated in the least-squares analysis. As a consequence, performing global fits over multiple doses and OH^- concentrations becomes essential to extract the necessary information. Use of lower OH^- concentrations makes the reaction 4 rate smaller. Hence, a significant fraction of the $H^\bullet$ atoms can react with e^-_{aq} via reaction 1 before being scavenged by OH^-, giving a fast decay or spike in the kinetics at early times. Using higher OH^- concentrations allows reaction 2 to dominate the kinetics. Variation of the H_2 concentrations used in these experiments was not found to greatly change the e^-_{aq} kinetics, as every H_2 concentration used put reaction 3 well within the pseudo-first-order limit where it exceeded the remaining reaction rates of interest.

Nonetheless, k_1 and k_2 are intimately coupled. If it is assumed that the e^-_{aq} decay is due only to reactions 1 and 2, then the decay can be written as

$$-\frac{d[e^-_{aq}]}{dt} = 2k_2[e^-_{aq}][e^-_{aq}] + k_1[H^+][e^-_{aq}] \qquad (5)$$

An equilibrium constant for reaction 4 can be written as

$$K_4 = \frac{[e^-_{aq}]}{[H^+][OH^-]} \qquad (6)$$

If we assume that this equilibrium is quickly established (in the present work, it occurs with a maximum time constant of 7 μs at 100 °C and 3.00×10^{-4} m OH^-),[6] then we can rearrange eq 6 for $[H^\bullet]$ and substitute into eq 5, giving

$$-\frac{d[e^-_{aq}]}{dt} = 2k_2[e^-_{aq}][e^-_{aq}] + \frac{k_1}{K_4[OH^-]}[e^-_{aq}][e^-_{aq}] \qquad (7)$$

Since we are in the pseudo-first-order limit of $[OH^-]$, we can write an effective second-order rate constant

$$k_{eff} = 2k_2 + \frac{k_1}{K_4[OH^-]} \qquad (8)$$

Consequently, we expect a second-order decay of e^-_{aq} whose rate constant depends on $[OH^-]$. At high $[OH^-]$, the second term in eq 7 becomes minimal. Therefore, k_1 and k_2 are more easily separated using multiple $[OH^-]$.

The early events of radiolysis leave a non-homogeneous mix of transient radical products in solution in pockets of high concentration, commonly referred to as spurs. Before diffusion allows these species to drift apart, the effective recombination rate is greater due to the locally high concentration. The radicals that diffuse out of the spurs without reacting are characterized by their escape yields, which are used as the starting point for the bulk homogeneous kinetics. The majority of the spur reactions tends to be completed within the first nanosecond following irradiation. (See ref 30 for an in-depth description of spur kinetics.) A stochastic radiation track simulation model[31−34] was applied to simulate the e^-_{aq} kinetics occurring within the first microsecond of production. Simulations were carried out for 250 bar, $[OH^-] = 3.0 \times 10^{-4}$ m, $[H_2] = 0.050$ m, and at temperatures coinciding with the experimental data. Figure 1 compares the e^-_{aq} kinetics obtained using our homogeneous kinetics model (4-ns radiolysis pulse, low dose) with the spur decay model at 150 °C. From this comparison, one can see that the majority of the spur chemistry is complete within the radiolysis pulse itself. However, a small tail persists for a few hundred nanoseconds after the pulse during which spur recombination chemistry still occurs. After this initial period, the shapes of the traces are identical.

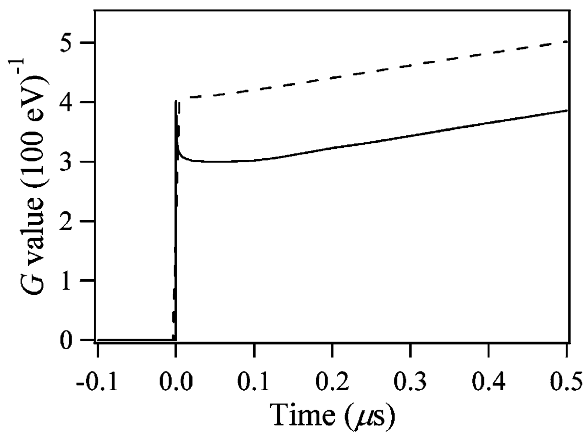

Figure 1. Time dependence of the hydrated electron yield as calculated with our homogeneous kinetic model (dashed line) alongside that obtained using the stochastic spur model of Pimblott and LaVerne[31−34] (solid line) for water at 150 °C, 250 bar, $[H_2] = 0.050$ m, and $[OH^-] = 3.0 \times 10^{-4}$ m. The homogeneous kinetic model does not incorporate spur chemistry. Using the spur model, one can observe that the majority of the spur decay is observed in the first few nanoseconds, but the spur chemistry subtly influences the kinetics out to hundreds of nanoseconds.

Given this long tail on the spur chemistry, we found it helpful to include a spur feature in our kinetic model to better replicate the time-dependent concentration profiles of both e^-_{aq} and $OH^•$. Since the stochastic model used to investigate the spur effects is computationally demanding, an approximated spur feature was used in our fitting code. It was assumed that the recombination of the electron due to spur reactions at these late times could be approximated by

$$S(t) = 1 + Ae^{-Bt} \tag{9}$$

where A is approximately 0.04 and B is approximately 5×10^6 s^{-1}. Assuming that the reaction of the electron with scavengers does not affect the decay of the electron (following similar assumptions used in Laplace transform techniques[35]), the pseudo-first-order decay rate constant at time t for the reaction of the electron due to spur processes is

$$k(t) = \frac{1}{S(t)}\frac{dS(t)}{dt} \tag{10}$$

This rate constant was then multiplied by the e^-_{aq} population and used as a decay term included in the overall reaction mechanism and fitting code. The values of A and B were varied to give the best agreement with the data. Using the spur decay term, the quality of the fits to individual traces and the fitted values of k_1 and k_2 were only very weakly dependent on the actual chosen values of A and B. Fitted values of k_1 and k_2 remained constant with changes in A and B of ±50%. However, the spur decay term did significantly improve the global fit quality, especially in calculating the overall dose dependence of the kinetics. Achieving credible global fits was nearly impossible before the inclusion of this spur ansatz. Therefore, inclusion of this approximated spur decay in the fitting model gives us more confidence in the quality of the reported values of k_1 and k_2. Parenthetically, it appears that the spur decay is far more important to include correctly at temperatures below 100 °C, which was not the primary target of this study. This would agree with expectations and the results of modeling, where diffusive escape wins over fast spur recombination in higher temperature water.

A related question is whether the presence of high H_2 concentrations may actually change the total effective escape yield of radicals normally input as constants in our kinetic model. Simulations were performed both in the presence of 0.050 m H_2 and in the complete absence of H_2 to observe the impact of the reaction 3 rate on the spur chemistry. A typical spur simulation at 150 °C is displayed in Figure 2. One can see in panel 2a that the product yields in the presence or absence of 0.050 m H_2 are almost identical up to 1 ns, at which point the majority of the spur chemistry has occurred. In panel 2b, it can be seen that even out to 1 μs, the total yield of all species differs negligibly in the presence or absence of H_2. This leads to the conclusion that reaction 3 is not fast enough to significantly affect the radical yields.

Experimentally, we found that high temperatures and large hydroxide concentrations cause corrosion, and hence higher ion concentrations, in the sample cell. Inductively coupled plasma atomic emission spectroscopy (ICP-AES) indicated levels of both Ni^{2+}_{aq} and Fe^{2+}_{aq} up to ~1 μM, depending on experimental conditions. Using a 1 μM concentration and a separate fitted rate constant on the order of 10^9 −to 10^{10}, a decay path due to impurities was added to our system of equations and used for all the fits. In most cases, the required decay rate due to impurities was small (ca. 10^3 s^{-1}), allowing our long-time scale

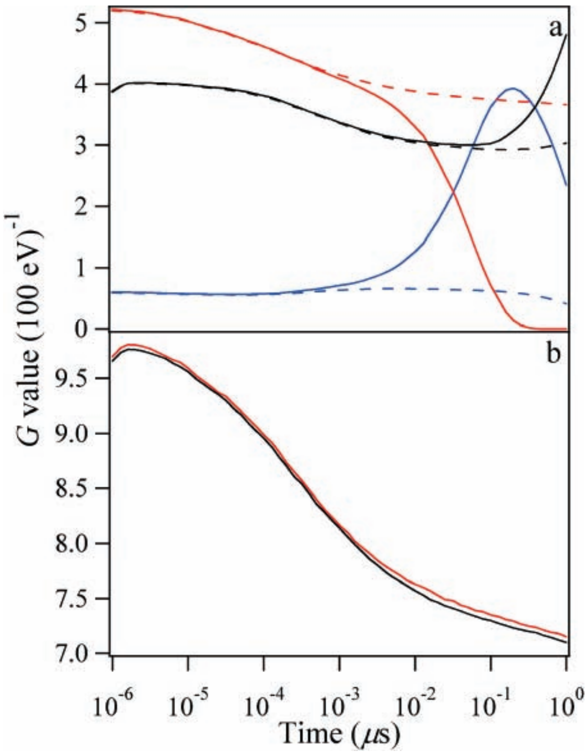

Figure 2. Calculated spur chemistry at 150 °C, 250 bar, and $[OH^-]$ = 3.0×10^{-4} m using the stochastic model,[31−34] showing radiation-induced product yields over the first 1 μs. (a) Solid lines are data calculated in the presence of 0.050 m H_2, and dashed lines are in the absence of any H_2. Red: $OH^•$; black: e^-_{aq}; and blue: $H^•$. (b) Sum of the yields of all species, $OH^• + e^-_{aq} + H^•$ for $[H_2]$ = 0.050 m (red) and 0 m (black).

fits to remain credible at least up to 250 °C. At higher temperatures, the impurity decay rate became as large as 5×10^4 s^{-1}, certainly destroying the credibility of our long-time scale fits where the decay rate merely due to reactions 1 and 2 is on a similar time scale.

Results

Typical experimental results and global fits to the kinetics are shown in Figure 3. Here, the transient absorption of e^-_{aq} at 950 nm at 175 °C and 250 bar is shown at a OH^- concentration of 0.0015 m. Experimental conditions for the data in Figure 3a−d are identical, except that the data in Figure 3a,b were acquired in the low-dose limit, and those in Figure 3c,d were acquired in the high-dose limit. Here, one can see the importance of acquiring data at multiple doses, as evidenced especially by Figure 3b,d. Low doses of radiation produce low transient concentrations, so low-dose data will tend to be dominated by first-order kinetics. At higher doses, the second-order reaction rates can begin to compete with the pseudo-first-order rates. At the low doses in Figure 3b, one can clearly see a ~1 μs growth of the signal after the prompt e^-_{aq} formation (at time zero) due to the e^-_{aq} production from reaction 4. With increasing doses, this feature is gradually buried due to the increasing importance of second-order reaction 1, and at the highest dose in Figure 3d, no signal growth can be seen. In Figure 3a,c, one can clearly see the long-time scale second-order e^-_{aq} decay due to reaction 2.

In Figure 4, one can observe the dependence of the e^-_{aq} kinetics on reaction 4. Here, the transient absorption of e^-_{aq} at 1050 nm at 250 °C and 250 bar is shown at OH^- concentrations of 1.0×10^{-4} m (Figure 4a,b) and 1.0×10^{-2} m (Figure 4c,d),

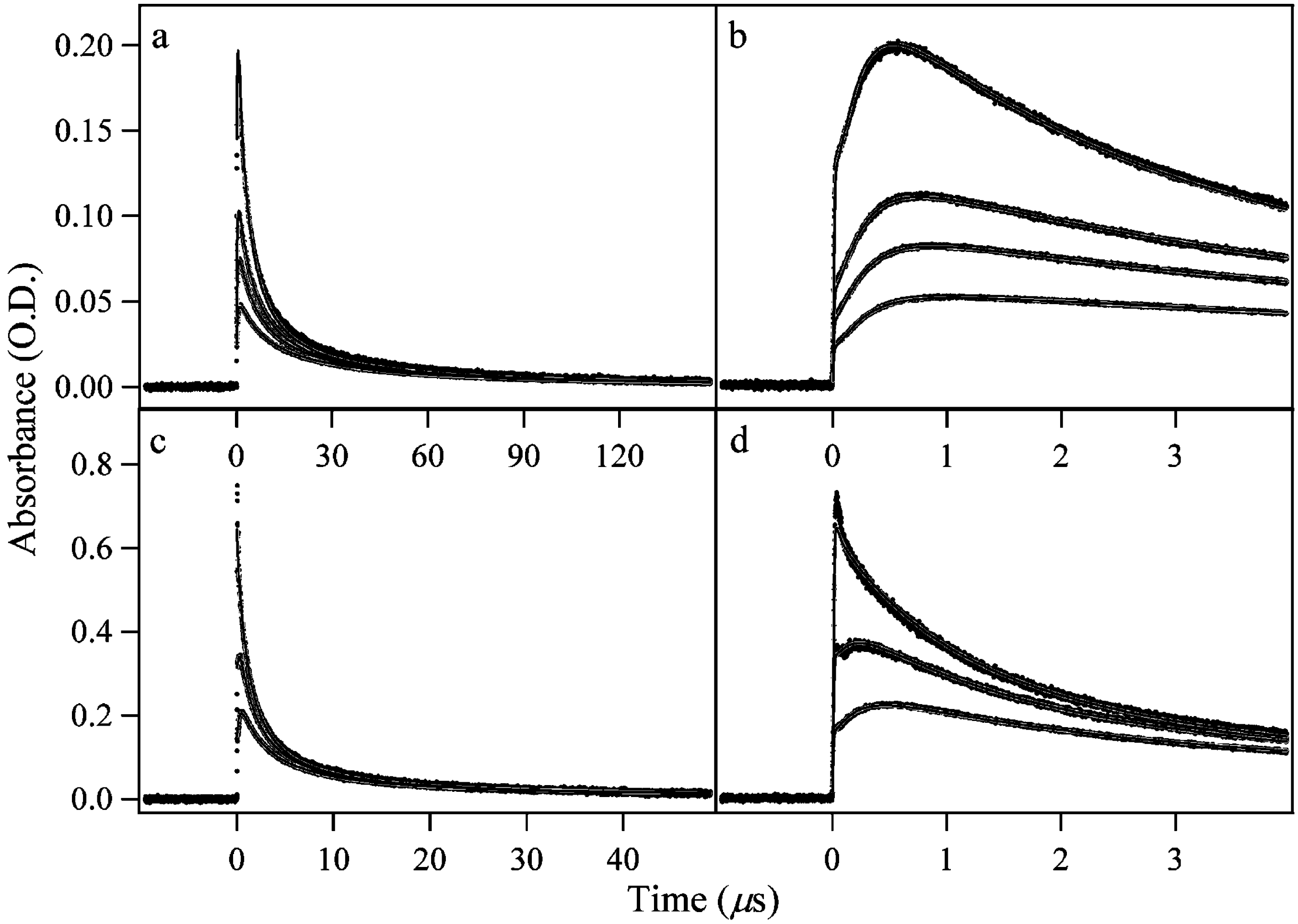

Figure 3. Transient absorption of e^-_{aq} (points) and global fits to the kinetics (solid lines) under multiple experimental conditions. Data in panels on the left and right are identical except for the time scale of data acquisition. The time scale has been adjusted in each panel to best visually present the data. Conditions for all data are 250 bar, 175 °C, $[OH^-] = 1.5 \times 10^{-3}$ *m*, $[H_2] = 0.037$ *m*, and 950 nm detection. Panels a and b illustrate data in the low-dose regime, and panels c and d illustrate data in the high-dose regime. Note the strong dose dependence on the shape of the kinetics.

respectively. A lower OH^- concentration favors the presence of $H^•$ atoms, and thus, in Figure 4a,b, the initial kinetics are dominated by reaction 1, and a large fraction of e^-_{aq} recombines with the $H^•$ atoms within a few microseconds. In contrast, in Figure 4c,d, one can see that with a factor of 100 greater OH^- concentration, the contribution of reaction 1 is minimal, and e^-_{aq} persists in a substantial concentration for hundreds of microseconds, following the predictions of eq 7.

In examining Figures 3 and 4, it is obvious that the global fits to the experimental data are reasonably good but not perfect. Near-perfect fits are achievable if performed on one trace at a time. However, this merely provides a range of values for k_1 and k_2 within a given data set, with the range of fitted values typically varying by ±15%. Performing global fits over multiple doses within a specific OH^- concentration proved to reliably produce k_1 and k_2 values that lie very close to an average of the values found with individual fits. Considering that the global fits achieve these values for a wide range of doses, this method of fitting was taken to be more reliable and was therefore used in analyzing all the results presented here. Global fits were carried out for all data acquired on a certain day for a given temperature, OH^- concentration, and dose regime (high-dose or low-dose limit). It became clear that where good global fits could not be obtained, there had been a problem with contaminants or corrosion in the sample cell, and these data were discarded. After cleaning and reconditioning the sample cell or replacing the inlet tubing, reacquired data always proved to give reliable results.

We attempted to perform global fits over both multiple doses and multiple OH^- concentrations. This exercise was a surprising failure, as the k_2 values seemed to display an inherent small (ca. 25% at most) dependence on the OH^- concentration. This trend is evident at least up to 200 °C. The value of k_1 was seemingly unaffected by changes in the OH^- concentration. Figure 5 shows the apparent dependence of k_2 on $[OH^-]$ for multiple temperatures. To test if this is some unexpected effect of ionic strength, data were acquired in the presence of 0.0015, 0.004, and 0.010 *m* $NaClO_4$ with a KOH concentration of 0.0015 *m* at 100, 200, and 275 °C. No change in the e^-_{aq} decay rate was observed, to within 1%.

Several equilibria of importance to water radiolysis are directly affected by pH, including those between $OH^•$ and $O^{•-}$, H_2O_2 and HO_2^-, and $HO_2^•$ and $O_2^{•-}$. Each of these was separately investigated within our fitting model to test its impact on the e^-_{aq} kinetics, but all of these species have concentrations that are too small to have a notable effect. The value of K_4 in eqs 6 and 7 certainly affects the fitted e^-_{aq} decay rate, particularly in the low-pH limit, where the second term in eq 7 attains a larger magnitude. In reviewing previous data for K_4,[36] we note that the error in its determination is estimated as ±30%. However, within these error limits, the fitted electron decay rate is changed by no more than a few percent. We estimate that an

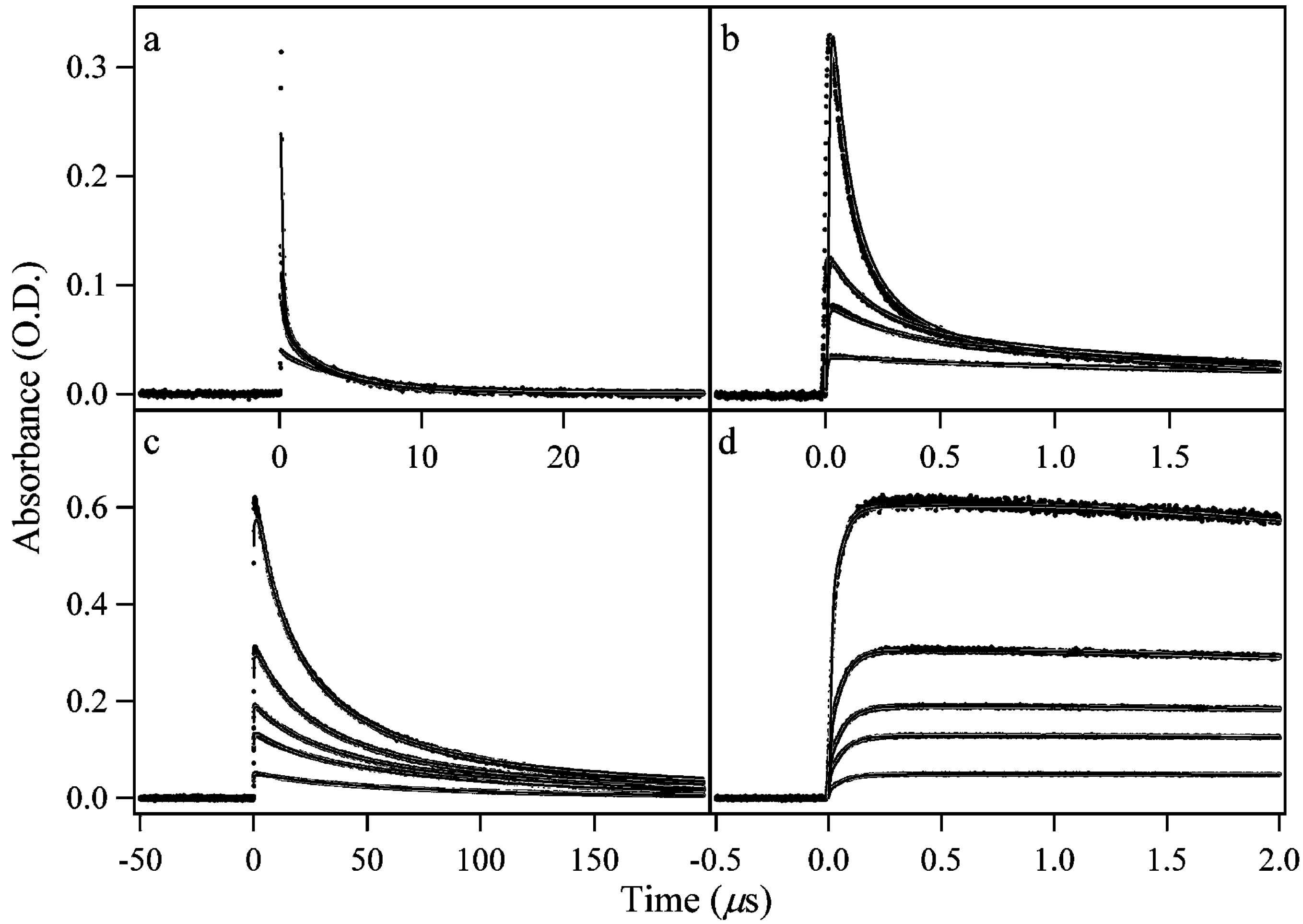

Figure 4. Transient absorption of e^-_{aq} (points) and global fits to the kinetics (solid lines) under multiple experimental conditions. Data in panels on the left and right are identical except for the time scale of data acquisition. The time scale has been adjusted in each panel to best visually present the data. Conditions for all data are 250 bar, 250 °C, and 1050 nm detection. A wide range of doses is applied. For panels a and b, $[OH^-] = 1.0 \times 10^{-4}$ *m*, and for panels c and d, $[OH^-] = 1.0 \times 10^{-2}$ *m*. Note not only the strong dependence of the kinetics on the applied dose but also on the hydroxide concentration.

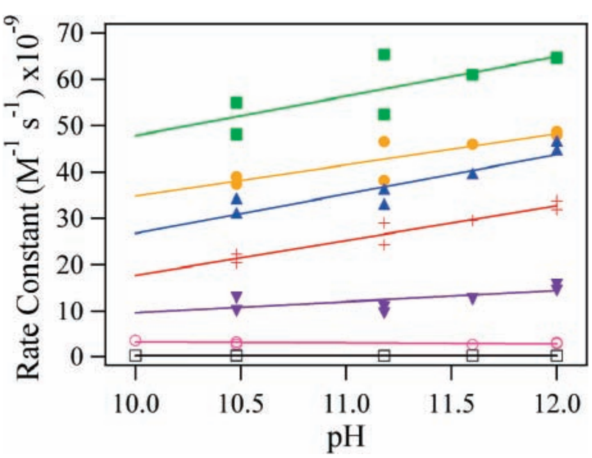

Figure 5. Dependence of the fitted value of k_2 on pH at multiple temperatures: 100 °C (red crosses), 125 °C (orange circles), 150 °C (green squares), 175 °C (blue triangles), 200 °C (inverted purple triangles), 225 °C (pink open circles), and 250 °C (black open squares). The fitted value of k_2 apparently increases at higher hydroxide concentrations. Virtually no pH dependence is observed above 200 °C. The linear fits to the data are in place merely to help guide the eye.

unreasonable factor of 5 decrease in the value of K_4 would be required to provide our observed pH effect.

With pH-sensitive equilibria and ionic strength effects discarded as causes for the pH dependence of k_2, we were forced to scrutinize our experimental conditions. The presence of impurities generated by corrosion in the sample cell and flow system is a very unlikely cause, as the pH effect is present even when corrosion is at a minimum. As stated previously, care was taken during data collection to ensure that impurities were not building up in the sample cell by applying cleaning pulses from the linac, causing any impurities to be chemically reduced. Regardless, an inorganic impurity has a high likelihood of surviving the radiation. The supplier of the KOH reagent used for these experiments claims that its heavy metal impurity levels should be ≤0.001%. Hence, for a 0.010 *m* KOH solution, a metal impurity concentration would be $\leq 10^{-7}$ *m*. Metal cations (M^{n+}) are well-known to react with e^-_{aq} on fast time scales. If we postulate a rate constant of 5×10^{11} M^{-1} s^{-1}, this could give a rate for the reaction of M^{n+} with e^-_{aq} in a 0.010 *m* KOH solution that falls within the domain of our experimental time scales and thus competes with the e^-_{aq} recombination until the ions are depleted. Such an effect would have the greatest influence at lower doses where the e^-_{aq} concentration is not large enough to overwhelm that of M^{n+}. For a lack of any other reasonable explanation, we propose impurities introduced with OH^- as the main source of the small pH dependence of k_2 shown in Figure 5. We reiterate that this represents a minor distortion of the kinetics and is only of concern because the data are so good.

Fitted values for k_1 and k_2 as a function of temperature are displayed in Table 1, where the values represent an average

TABLE 1: Fitted Values for Rate Constants k_1 and k_2 as a Function of Temperature[a]

temp (°C)	k_1 (M^{-1} s^{-1})	k_2 (M^{-1} s^{-1})
100	$9.31 \pm 0.84 \times 10^{10}$	$2.73 \pm 0.50 \times 10^{10}$
125	$1.17 \pm 0.06 \times 10^{11}$	$4.34 \pm 0.50 \times 10^{10}$
150	$1.49 \pm 0.12 \times 10^{11}$	$5.87 \pm 0.69 \times 10^{10}$
175	$1.95 \pm 0.11 \times 10^{11}$	$3.76 \pm 0.59 \times 10^{10}$
200	$2.47 \pm 0.13 \times 10^{11}$	$1.27 \pm 0.23 \times 10^{10}$
225	$3.40 \pm 0.23 \times 10^{11}$	$3.19 \pm 0.70 \times 10^{9}$
250	$4.60 \pm 0.38 \times 10^{11}$	$3.83 \pm 0.81 \times 10^{8}$
275	$6.28 \pm 0.79 \times 10^{11}$	3.36×10^{8}
300	$7.68 \pm 0.79 \times 10^{11}$	4.98×10^{8}
325	$1.17 \pm 0.16 \times 10^{12}$	

[a] Note that data for k_2 at 275 and 300 °C should merely be considered upper limits for its true value.

TABLE 2: Fitted Average Values of k_2 Obtained under Different Temperatures and OH^- Concentrations

	[OH^-] (*m*)				
temp (°C)	1.0×10^{-4}	3.0×10^{-4}	1.5×10^{-3}	4.0×10^{-3}	1.0×10^{-2}
100		2.14×10^{10}	2.67×10^{10}	2.95×10^{10}	3.25×10^{10}
125		3.82×10^{10}	4.24×10^{10}	4.60×10^{10}	4.84×10^{10}
150		5.15×10^{10}	5.89×10^{10}	6.10×10^{10}	6.45×10^{10}
175		3.24×10^{10}	3.43×10^{10}	3.94×10^{10}	4.54×10^{10}
200		1.19×10^{10}	1.07×10^{10}	1.30×10^{10}	1.55×10^{10}
225	3.66×10^{9}	3.09×10^{9}		2.74×10^{9}	3.11×10^{9}
250	3.70×10^{8}	3.83×10^{8}	3.54×10^{8}	4.06×10^{8}	3.66×10^{8}

over multiple hydroxide concentrations. The uncertainty placed on the listed values incorporates the relative standard deviation (rsd) of the global fitted values for all the data sets acquired at a particular temperature and all hydroxide concentrations. Thus, the uncertainty in k_2 incorporates the dependence on the pH. Above 200 °C, additional uncertainty beyond the rsd is also incorporated to account for the implications of sample impurities. At all the temperatures measured, no fitted value for k_2 deviates from the average value for all OH^- concentrations by more than 25%. Values for k_2 at 275 and 300 °C could not be reliably fit due to significant corrosion impurity levels. However, the values listed in Table 1 at these temperatures can be considered as upper limits for the true rate constant.

Table 2 lists the average values of k_2 obtained at each different OH^- concentration and temperature. All fitted values for k_1 and k_2 for individual fitted data sets are included as Supporting Information. Note that all the rate constant values have been properly adjusted for changes in the e^-_{aq} maximum extinction coefficient (ϵ) as a function of temperature (the actual fitted numbers are k_2/ϵ). The extinction coefficient can be described as (in units of M^{-1} cm^{-1})

$$\epsilon(T) = 1.741 \times 10^{-4}T^3 - 1.949 \times 10^{-2}T^2 - 6.736T + 1.858 \times 10^4 \quad (11)$$

where T is in degrees Celsius for temperatures up to 325 °C. The e^-_{aq} extinction coefficient was obtained by integrating the e^-_{aq} spectrum at each temperature, under the assumption that the absorption oscillator strength is conserved at all temperatures. These were then normalized to the integral of the spectrum at 25 °C. The temperature dependence of the e^-_{aq} absorption spectrum was addressed in a recent publication.[26] Those data were combined with the low-temperature data of Jou and Freeman[37] to give eq 11.

Arrhenius plots for k_1 and k_2 are shown in Figures 6 and 7, respectively. Previously reported data are overlaid in these figures, where the rate constants have been corrected for the new electron extinction coefficients. Previous measurements of

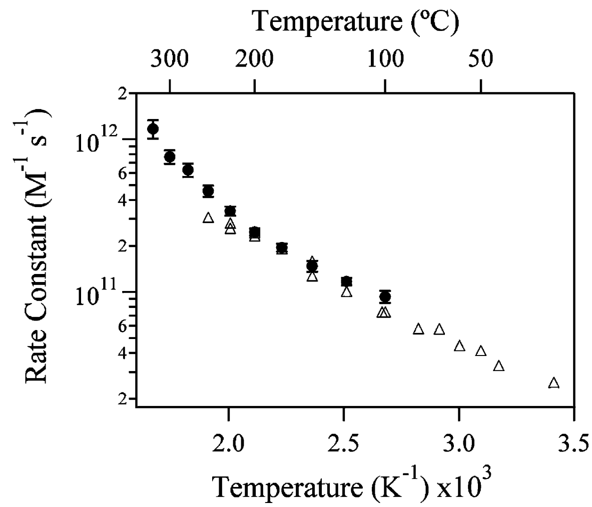

Figure 6. Arrhenius plot for reaction 1 showing the averages of the current data across all measured OH^- concentrations (circles) and previous data from ref 10 (triangles).

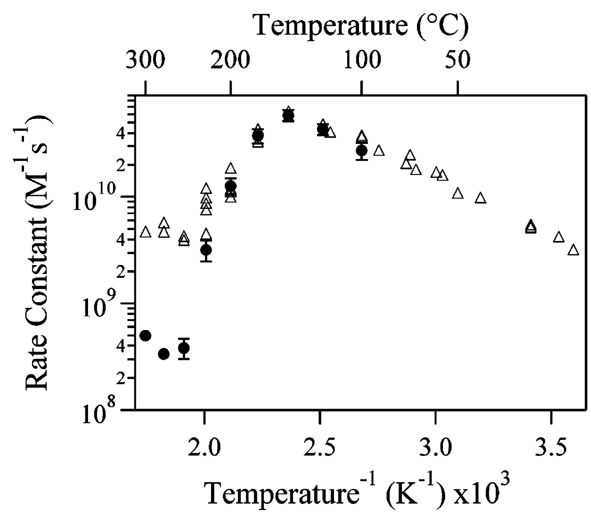

Figure 7. Arrhenius plot for reaction 2 showing the averages of the current data across all measured OH^- concentrations (circles) and previous data from ref 17 (triangles).

k_1 showed Arrhenius behavior up to 250 °C with an activation energy of 14 kJ mol^{-1}.[10] In Figure 6, these data can be seen to agree reasonably well with the current data up to 200 °C. With the two data sets combined, k_1 displays an activation energy that continually increases with increasing temperature, from 14 kJ mol^{-1} at 100 °C ($k_1 = 9.3 \times 10^{10}$ M^{-1} s^{-1}) up to 34 kJ mol^{-1} at 325 °C ($k_1 = 1.2 \times 10^{12}$ M^{-1} s^{-1}). If we ignore previous data collected above 200 °C, a polynomial fit to the combined current and previous data provides the expression, where T is in Kelvin

$$\log(k_1) = -1.9651 \times 10^8\left(\frac{1}{T}\right)^3 + 1.7914 \times 10^6\left(\frac{1}{T}\right)^2 - 6.0997 \times 10^3\left(\frac{1}{T}\right) + 1.8146 \times 10^1 \quad (12)$$

which can be used to simulate the data up to 325 °C.

Rate constant k_2 shows a similar behavior to that previously reported,[17] showing basically Arrhenius behavior up to 150 °C with an activation energy of 20 kJ mol^{-1}, similar to the previously reported value of 23 kJ mol^{-1}. It reaches a maximum value of 4.5×10^{10} at 150 °C and above this temperature declines in value. Above 250 °C, the k_2 value is too small to measure reliably with our experiments, so again the data shown at 275 and 300 °C should be regarded as upper limits for the rate constant. Overall, the values for k_2 agree with those previously reported up to 200 °C if those results are adjusted for the e^-_{aq} extinction coefficient as outlined previously. A polynomial fit to the current data and data at $T \leq 200$ °C from ref 17 provides the expression (with T in K)

$$\log(k_2) = 1.0427 \times 10^{15}\left(\frac{1}{T}\right)^5 - 1.6876 \times 10^{13}\left(\frac{1}{T}\right)^4 + 1.0849 \times 10^{11}\left(\frac{1}{T}\right)^3 - 3.4641 \times 10^{8}\left(\frac{1}{T}\right)^2 + 5.4841 \times 10^{5}\left(\frac{1}{T}\right) - 3.3303 \times 10^{2} \quad (13)$$

which can be used to simulate the data from 5 to 250 °C.

Whereas the trend shown in the current data for k_2 as a function of temperature is very similar to that previously obtained by Christensen and Sehested,[17] the actual values obtained above 200 °C are significantly smaller (see Figure 7). Furthermore, where in the previous study measurement was possible up to 300 °C, the current data show no leveling off of the rate constant at high temperature but rather a steady steep falloff to the point where it has become too small in value to measure above 250 °C. The lifetime of the hydrated electron is not only limited by reactions 1 and 2 but also by the contribution of impurities in the sample. It was acknowledged by the previous authors that a significant silicate concentration was present in their samples, especially at high temperatures, due to dissolution of their quartz sample cell. The transformation of the silica sample cell to aqueous silicic acid had the effect of lowering the sample pH, which would decrease the observed electron lifetime due to the impact of reaction 1. This would have the overall effect of increasing the fitted k_2 values if the sample pH was not properly accounted for. The fact that the current data show a smaller rate constant could reflect an overall much smaller impurity level in the sample.

In the current high-temperature data above 250 °C, it is obvious that impurities were causing a significant amount of the e^-_{aq} decay, as a pure second-order decay is no longer observed. Hence, our fitted k_2 values above 250 °C are merely reported as upper limits for the true k_2 value. Nevertheless, the observed electron lifetime is far longer than that observed by Christensen and Sehested at all temperatures >200 °C,[17] leading us to believe that their high-temperature data are unreliable due to impurities. The exact nature and implications of the present impurities needs to be further investigated.

Discussion

Rate Constant for H$^\bullet$ + e$^-_{aq}$. *Application of the Smoluchowski Equation.* The rate of reaction 1 is very high, and the first question to address is to what extent diffusion limits the reaction. The rate constant for a diffusion-controlled reaction is described by the Smoluchowski equation

$$k_{diff} = 4\pi\sigma\beta R(D_a + D_b) \quad (14)$$

where D_a and D_b are the diffusion coefficients of the reactants, R is the reaction distance, and β is a spin statistical factor, usually set to unity but equal to 1/4 for reacting doublets. The term σ is set to 1/2 if the reactants are identical (to avoid counting encounters twice) but is unity otherwise.

Information on the H$^\bullet$ atom diffusion coefficient and radius has been explicitly determined only at room temperature,[38] although the rate constant for the diffusion-limited bimolecular recombination of the H$^\bullet$ atom also implies its diffusion coefficient, and this information is available up to 250 °C.[39] Elliot demonstrated that this rate constant scales with water self-diffusion above room temperature, at least to within the signal-to-noise ratio of the data.[29] On the basis of this information, we will assume that its room-temperature diffusion coefficient of 7.0×10^{-9} m^2 s^{-1} scales the same as the water diffusion coefficient.[40] Hence, we describe the H$^\bullet$ atom diffusion coefficient as

$$D_H = 7.0 \times 10^{-9}\,\frac{D_{H_2O}(T)}{D_{H_2O}(25\ °C)} \quad (15)$$

We should note that the H$^\bullet$ atom bimolecular recombination rate constant data are reported as $2k/\epsilon$ (where ϵ is for the H$^\bullet$ atom), and the values used for ϵ may be slightly underestimated at high temperatures. In this case, the H$^\bullet$ atom diffusion coefficient would have a slightly larger temperature coefficient than indicated. On the basis of the data analysis of ref 2, the H$^\bullet$ atom bimolecular recombination and diffusion coefficient will be underestimated by no more than 50% at 350 °C. We further assume that the H$^\bullet$ atom radius is a constant 1.9 Å.[38]

The temperature dependence of the e^-_{aq} radius of gyration was recently determined from moment analysis of the e^-_{aq} absorption spectrum[41] and can be described by

$$r_{e^-_{aq}} = 2.4038 + 9.668 \times 10^{-4}T + 1.1294 \times 10^{-5}T^2 - 1.1348 \times 10^{-8}T^3 \quad (16)$$

where T is in degrees Celsius, and the resulting radius is in angstroms. The e^-_{aq} diffusion coefficient is known to be 4.8×10^{-9} m^2 s^{-1} at room temperature[42] and was previously studied up to 90 °C by Schmidt et al.[43] It displayed Arrhenius behavior above room temperature with a large activation energy of 20.25 kJ mol^{-1}. An equation describing the e^-_{aq} diffusion coefficient was provided

$$\log D_{e^-} = -4.7644 - \frac{1058.18}{T} - \left(\frac{259.12}{T}\right)^{50} \quad (17)$$

where T is in Kelvin, and D is in square meters per second. As seen in Figure 7, reaction 2 displays Arrhenius behavior up to 150 °C with a very similar activation energy of 19.8 kJ mol^{-1}, so we can assume that eq 17 holds true at least up to 150 °C. Previous measurements of e^-_{aq} scavenging by nitrobenzene showed approximate Arrhenius behavior up to 300 °C with an average activation energy of 20.8 kJ mol^{-1}.[25] Since the e^-_{aq} diffusion is rate limiting for this reaction, it was suggested that the activation energy was due solely to e^-_{aq} diffusion. Thus, we begin with the assumption that eq 17 gives a reasonable estimate of the e^-_{aq} diffusion coefficient up to 300 °C.

With diffusion coefficients for both e^-_{aq} and H$^\bullet$ and fitted rate constants for reaction 1 in hand, one can calculate a reaction distance for reaction 1 using eq 14. For two reacting doublets, β takes on a value of 1/4. The calculated value of R as a function of temperature is shown in Figure 8. The reaction distance decreases with temperature up to 200 °C, and then increases with temperature up to 300 °C. This is compared to an estimate of the contact distance, the sum of the individual radii of both e^-_{aq} and H$^\bullet$, where the e^-_{aq} radius of gyration versus temperature is taken from ref 26, and the H$^\bullet$ radius is taken to be a constant 1.9 Å.[38] It can be seen that the reaction distance substantially exceeds the estimated contact distance at all temperatures.

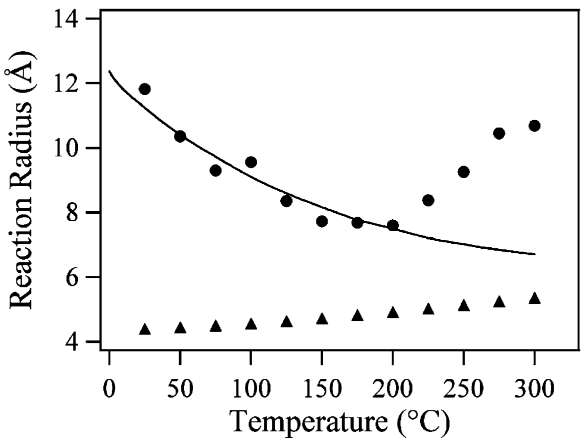

Figure 8. Calculated value of the reaction distance for reaction 1 as a function of temperature (circles) and sum of the $H^{\bullet}$ atom and e^-_{aq} radii (triangles), where we have solved for R in the Smoluchowski equation. The line represents a best fit to the reaction distance using the described ET mechanism within the radiation boundary condition.

Hence, reaction 1 seems to be a long-range electron transfer (ET) reaction.

ET Model. It is an open question as to whether standard Marcus ET theory can handle a highly polarizable species such as the hydrated electron. Lacking a better model, we will apply the standard framework to gain at least qualitative insight into the reaction 1 reaction distance. In particular, we seek to investigate why the reaction distance should decrease and then increase with temperature.

Long-range ET reactions such as reaction 1 have been addressed previously in the context of extended Marcus theory and the Smoluchowski equation by using a radiation boundary condition.[44,45] The result of Marcus theory and its extensions incorporating quantum vibrational degrees of freedom is an ET rate expression taking the form[46−50]

$$W(R_{ET}, T) = \frac{H_{ab}^{\ 2}}{\hbar}\left(\frac{\pi}{\lambda k_B T}\right)^{1/2} \sum_{n_f} e^{-S}\frac{S^{n_f}}{n_f!} \exp\left[-\frac{(\Delta_r G + \lambda + n_f h\nu)^2}{4\lambda k_B T}\right] \quad (18)$$

where λ is the solvent reorganization energy, H_{ab} is the electronic coupling matrix element for reactants a and b, and $\Delta_r G$ is the free energy of the ET reaction. The weighted sum is termed an effective Franck−Condon density of states for the acceptor ground state with the vibrationally excited state of the product and is taken over quantized vibrational states of the product with energies $n_f h\nu$. The S terms are Huang−Rhys electron-vibration coupling constants for each vibrational mode where $S = \Delta^2/2h$, and Δ is the dimensionless mode displacement. $W(R_{ET}, T)$ is dependent on the ET distance R_{ET} through the coupling matrix element, which behaves exponentially as

$$H_{ab}^{\ 2} = \alpha_{ET} \exp(-\beta_{ET}[R_{ET} - R_0]) \quad (19)$$

Here, α_{ET} is the coupling matrix element for a donor−acceptor pair at van der Waals separation R_0, and β_{ET} is a constant scaling the ET distance dependence. The distance dependence of the rate is also manifested through the reorganization energy. Assuming spherical initial (i) and final (f) states, the solvent reorganization energy can be expressed as[51]

$$\lambda = \left(\frac{1}{\epsilon_{opt}} - \frac{1}{\epsilon_s}\right)\left(\frac{1}{2r_i} + \frac{1}{2r_f} - \frac{1}{R_{ET}}\right) \quad (20)$$

where ϵ_{opt} and ϵ_s are the optical and static dielectric constants of the solvent, respectively. The term ϵ_{opt} is normally approximated as the square of solvent refractive index for visible light. (The refractive index at a wavelength of 700 nm is chosen here, with data taken from ref 52.)

As is well-known, the ET rate constant will be maximized for a given distance R when the reaction free energy $\Delta_r G$ is equal in magnitude but of opposite sign to the reorganization energy. If one assumes that reaction 1 is actually a two-step process

$$H^{\bullet} + e^-_{aq} \rightarrow H^- \quad (1a)$$

$$H^- + H_2O \rightarrow H_2 + OH^- \quad (1b)$$

then a free energy for the ET in reaction 1a can be calculated from the Gibbs energies of formation of the species involved via

$$\Delta_r G = \Delta_f G(H^-_{aq}) - \Delta_f G(H^{\bullet}_{aq}) - \Delta_f G(e^-_{aq}) \quad (21)$$

where $\Delta_f G(H^{\bullet}_{aq})$ is the sum of the gas phase Gibbs energy $\Delta_f G(H^{\bullet}_{gas})$ and the hydration free energy. It has been demonstrated[53] that H_2 solubility data[54] provide a good approximation to the latter quantity. Temperature dependence of $\Delta_f G$ for e^-_{aq} can be obtained from Bartels et al.[26] $\Delta_f G$ for the postulated aqueous hydride intermediate is available only at room temperature from recent calculations by Kelly and Rosseinsky, with a value of 141 kJ mol^{-1}.[55] The $\Delta_f G$ for other aqueous anions is known to be relatively temperature-insensitive,[26] and consequently, we assume that this value holds constant over our temperature range of interest. The resulting $\Delta_r G$ indicates a near-constant −3.7 eV change in free energy over the entire experimental temperature range.

Reaction 1a apparently has no internal reorganization energy to speak of since there should be no high-frequency vibrational modes to consider for the H^- product. Consequently, it is appropriate to discuss this reaction in the context of classical Marcus theory and drop the sum over vibrational states in eq 18. Using eq 20 to describe the solvent reorganization energy, the parameter r_i is taken to be the electron radius of gyration r_g (measured via integration of its absorption spectrum), and r_f is taken to be 1.38 Å.[55] For the entire temperature range of interest, we find $-\lambda = \Delta_r G$ for values of R_{ET} in the 1.1−1.4 nm range, so that the reaction must be occurring (cf. Figure 8) with a near optimum ET rate. In Figure 9, we plot the Marcus rate expression versus the ET distance R_{ET} for several temperatures spanning our temperature range, where we assume a typical overlap integral with $\beta_{ET} = 1.0$ Å^{-1}. The overall reaction probability versus distance deviates only slightly from exponential until R_{ET} is nearly at the contact distance (∼4.8 Å) and is nearly independent of temperature.

The combined diffusion- and distance-dependent reaction rate can be solved in the framework of the Smoluchowski equation by invoking the radiation boundary condition.[44,45] An exponential distance dependence is assumed for the ET probability, $p(R) = \alpha_{ET} \exp(-\beta_{ET} R)$ (i.e., the behavior of $H_{ab}^{\ 2}$, same as in eq 19 but with $R_0 = 0$), and R is replaced by

$$R^* = \frac{2}{\beta_{ET}}\left[\gamma + \ln\left[\frac{1}{\beta_{ET}}\left(\frac{\alpha_{ET}}{D}\right)^{1/2}\right] + \frac{K_0(x) - yK_1(x)}{I_0(x) - yI_1(x)}\right] \quad (22)$$

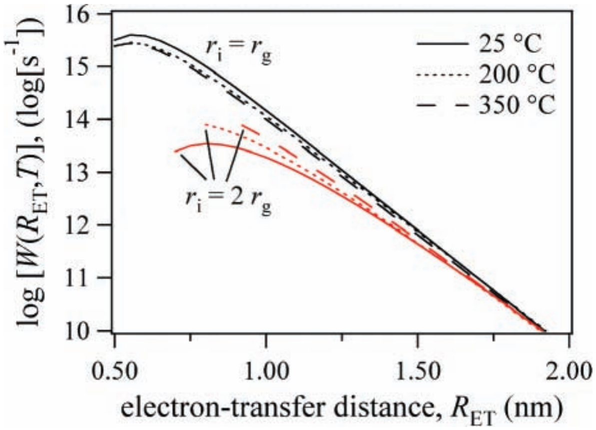

Figure 9. Calculated Et rate $W(R_{ET}, T)$ for reaction 1 at several temperatures, as a function of the ET distance R_{ET} between $H^•$ and e^-_{aq}. Upper curves are for initial (hydrated electron) radius r_i equal to the radius of gyration r_g. Lower curves use the assumption $r_i = 2r_g$. For $r_i = r_g$, the overall reaction probability vs distance deviates only slightly from exponential until R_{ET} is nearly at the contact distance (~4.8 Å) and is nearly independent of temperature. When we double the electron radius to $2r_g$, a stronger distance dependence emerges.

with

$$x = \frac{1}{\beta_{ET}}\left(\frac{\alpha_{ET}}{D}\right)^{1/2} \exp\left(-\frac{a\beta_{ET}}{2}\right) \text{ and } y = \frac{ax\beta_{ET}}{2}$$

Here, a is the diffusional distance of closest approach, γ is Euler's constant, and $I_{0,1}$ and $K_{0,1}$ are modified Bessel functions of the first and second kind, respectively. In finding a fit to the R values in Figure 8, we arrive at $\alpha_{ET} = 4.5 \times 10^{13}$ s^{-1} and $\beta_{ET} = 1.3$ Å^{-1} for the data up to 200 °C. This β_{ET} value is fairly typical for ET problems. The data above 200 °C cannot be fit within the confines of this model. No physical values of α_{ET} and β_{ET} allow for an increase in reaction radius, even if a reasonable temperature dependence is allowed for.

We also considered that the choice of r_i set equal to the electron radius of gyration r_g may be an underestimate. Doubling this electron radius reduces the reorganization energy and puts the ET reaction into the Marcus inverted region at all temperatures and distances. The result of the Marcus expression in this approximation is also plotted in Figure 9. It can be seen that the predicted ET rates are lower, and the exponential distance dependence is somewhat distorted. Nevertheless, such a choice of parameters cannot yield a significant increase in average reaction distance with temperature. We conclude that according to the Marcus ET model, the average reaction distance should continue to decrease above 200 °C.

High-Temperature Diffusion Coefficients. Because the Marcus theory does not predict that the reaction radius could increase sufficiently to explain the rate data, it is necessary to explore whether the diffusion coefficients of the reactants could be responsible. It is possible that the reaction distance is not, in fact, increasing, but that at high temperatures, the diffusion coefficients of the reactants are increasing more rapidly than estimated, so that we have incorrectly inferred the reaction distance. Inspection of Figure 8 suggests that at 300 °C, the relative diffusion coefficients of $H^•$ and e^-_{aq} would need to be twice as large as our extrapolation from lower temperature predicts.

Both $H^•$ and e^-_{aq} diffusion coefficients are predicted to be of similar magnitude above 200 °C (although e^-_{aq} is larger), and it is not immediately obvious which extrapolated value is too low to explain the temperature dependence of k_1. The $H^•$ atom data are constrained by the measured reaction rate for $H^• + H^• \rightarrow H_2$, which must certainly be diffusion-limited. Values of $2k/\epsilon$ have been measured for this reaction up to 250 °C,[39] but the values for ϵ are in some doubt. Our recent analysis of data for the $H^• + O_2$ reaction rates[2] could be consistent with a 50% larger $H^• + H^•$ reaction rate at 325 °C. This is entirely possible within the confines of our fitting model for k_1 and k_2, as a 50% increase in the $H^• + H^•$ rate constant has a very modest effect on the fitted k_1 value, causing it to increase by no more than 15%. This is almost within the range of our fitting error limits and thus leaves the e^-_{aq} diffusion as responsible for the greater part of the discrepancy in our diffusion coefficients. Assuming that eq 17 (20 kJ mol^{-1} activation energy) is correct up to 125 °C, we can approximately account for the data in Figure 8 if the activation energy for electron diffusion then increases to about 32 kJ mol^{-1}. This gives a factor of 3 larger diffusion coefficient for e^-_{aq} at 300 °C (i.e., 2.4×10^{-7} m^2 s^{-1}) than extrapolated from lower temperatures.

The upper limit for e^-_{aq} diffusion should be constrained by the reaction rate data for nitrobenzene[25] mentioned earlier. Given the large negative free energy change, this reaction ought to be diffusion-limited and have a decreasing reaction distance at elevated temperature very similar to reaction 1. From the measured rate constants of ref 25, we estimate that a diffusion-limited nitrobenzene reaction might easily be consistent with a factor of 2 larger diffusion rate for e^-_{aq} at 300 °C. The factor of 3 increase in diffusion required previously would imply that the nitrobenzene reaction is no longer diffusion-limited above about 250 °C. This result, if correct, is surprising but not impossible. Conductivity measurements of the e^-_{aq} mobility at high temperature are planned to resolve this issue.

In conclusion, it would appear that the hydrated electron diffusion coefficient, already abnormally large at room temperature,[42] must become much larger than that of a classical object of similar size at elevated temperatures, to explain the rate constant for reaction 1. It represents a challenge for theoreticians and modelers to explain and reproduce this behavior.[56] A further implication is that diffusional escape from geminate or spur recombination will be greatly enhanced at elevated temperatures.

Rate Constant for $e^-_{aq} + e^-_{aq}$. The second-order reaction of hydrated electrons has been a subject of puzzlement for many years. The first study of this reaction dates back over 40 years,[18] and several other studies have followed.[11,13−21,23,24,43] Certainly, the most comprehensive of these was conducted by Christensen and Sehested, whose results did not differ greatly from the work presented here.[17,57] Their data show very similar non-Arrhenius behavior to the current results, and they suggested a mechanism for the formation of an intermediate dielectron ($e_2{}^{2-}{}_{aq}$) as an explanation, where reaction 2 is really a two-step process

$$e^-_{aq} + e^-_{aq} \leftrightarrow e_2{}^{2-}{}_{aq} \tag{2a}$$

$$e_2{}^{2-}{}_{aq} \rightarrow H_2 + 2OH^- \tag{2b}$$

The argument for the turnover in the Arrhenius plot is the existence of equilibrium 2a. It was suggested that the reverse rate constant k_{-2a} is low at room temperature but has a high activation energy as compared to k_{2a} and thus competes with k_{2b} at higher temperatures. Our new data add little to this analysis, except to clarify the degree to which the reaction turns off above 150 °C.

It was argued by Han and Bartels[57] that reaction 2b might in itself be a two-step reaction involving a proton transfer

$$e_2{}^{2-}{}_{aq} + H_2O \rightarrow H^- + OH^- \quad (2b1)$$

$$H^- + H_2O \rightarrow H_2 + OH^- \quad (1b)$$

When reaction 2 is conducted in the presence of isotopically mixed water, the H_2 product is greatly favored over HD or D_2.[58] This might suggest that an intermediate species (i.e., $e_2{}^{2-}{}_{aq}$) lives long enough to wait for contact with an H-bearing water molecule to facilitate proton transfer.

A room-temperature study of reaction 2 by Schmidt and Bartels[22] in the presence of large concentrations of $LiClO_4$ indicated no notable ionic strength effect, confirming the lack of an ionic strength effect in the experiments of Christensen and Sehested. Using measured diffusion and reaction rates, with a spin factor of 1/4, the Debye−Smoluchowski equation leads to an estimated reaction distance of 9 Å. Given this large reaction distance, the rate acceleration expected from the kinetic salt effect is counterbalanced by added solvent friction, lessening the $e^-{}_{aq}$ diffusion rates. The reaction distance does not decrease with faster diffusion at elevated temperatures as observed in Figure 8 for reaction 1. Apparently, the mechanism does not involve a long-range ET. The reaction distance of 9 Å suggests that a solvent-separated electron pair might be barely thermodynamically stable around this threshold distance. The assumption of Schmidt and Bartels was that the dielectron would then inevitably form, with spin-paired electrons sharing the same solvent cavity. The proton transfer of reaction 23 would quickly follow.

The unambiguous existence of aqueous dielectrons has yet to be determined experimentally. Recent simulations of the dielectron by Larsen and Schwartz confirm the long-held suspicion that a dielectron should absorb in the same spectral region as single electrons (although slightly shifted to the blue) and with nearly twice the oscillator strength.[59] This will make them difficult to detect given their short lifetime and inherently low concentration but perhaps not impossible in femtosecond laser experiments.[60,61] More troublesome is the finding that spin-paired electrons solvated within a single cavity are thermodynamically unstable by 2.6 eV with respect to a pair of separated electrons.[62] This would seem to rule out a diffusion-limited reaction as observed and casts immediate suspicion on the adequacy of the simulation model (two quantum electrons within classical MD water.) However, the model would need to be extremely bad to obtain a result in error by this amount. Very recent simulations of the potential of mean force separating a pair of solvated electrons[63] found a solvent-separated free energy minimum at a distance of ca. 7 Å.

So how can this reaction occur? Perhaps the data collected on reaction 1 taken together with the dielectron simulation provide enough insight to synthesize a new mechanism. Suppose that proton transfer occurs to one of the electrons of the slightly stabilized solvent-separated electron pair (at 9 Å) to form an $H^\bullet$ atom and OH^-. We can postulate that the strong electric field engendered by the close proximity of two electrons makes this proton transfer nearly certain on the time scale of the diffusive encounter. According to Figure 8, this would place the $H^\bullet$ atom and the remaining electron within the effective reaction distance for reaction 1 even up to 150 °C, and long-range ET should occur with unit probability to form H^-, followed by conversion to H_2 and OH^-. At temperatures above 150 °C, the solvent-separated electron pairs may become less stable, and the proton-transfer step may become less probable, which would explain the drop in reaction rate at higher temperatures. This mechanism may also explain the lack of observation of the dielectron spectrum in femtosecond laser experiments because no spectral blue shift corresponding to electrons in the same cavity would ever be present. The strong H/D isotope effect, which is the strongest evidence for the existence of an intermediate of finite lifetime in reaction 2, could still come from the initial proton-transfer step in a solvent-separated pair.

Conclusion

Rate constants for the reaction of hydrated electrons with hydrogen atoms (k_1) and the bimolecular reaction of two hydrated electrons (k_2) were measured over the temperature ranges of 100−325 and 100−250 °C, respectively. Both rate constants show non-Arrhenius behavior over the entire temperature range studied. k_1 values agree well with previous studies up to 200 °C, but at higher temperatures, the activation energy increases with temperature. Analysis of this reaction rate via the Smoluchowski equation suggests that the reaction is a long-range ET. The rapidly increasing reaction rate above 200 °C suggests that hydrated electron diffusion increases much more than expected. The general trend of k_2 as a function of temperature has been reconfirmed. The k_2 value increases with the diffusional activation energy of 20 kJ mol^{-1} up to 150 °C. Above this temperature, it rapidly decreases in value. In light of recent modeling studies, we suggest that the first step of the reaction is a proton transfer stimulated by the proximity of the two electrons. The hydrogen atom so formed is already within the reaction radius for reaction 1 to occur as the second step.

Acknowledgment. We thank Dr. Simon M. Pimblott of the University of Manchester for aid in the calculations of the spur kinetics. We also acknowledge Dr. Lisa M. Utschig of the Argonne National Laboratory for her assistance with the ICP-AES measurements. Work was performed at the Argonne National Laboratory (Contract W-31-109-ENG-38) under the auspices of the Office of Science, Division of Chemical Science, U.S. DOE. Additional funding for K.T. and T.W.M. was provided by the U.S. DOE Nuclear Energy Research Initiative Grants 99-276 and 02-060. This is Document NDRL-4731 from the Notre Dame Radiation Laboratory.

Supporting Information Available: Table of fitted rate constants k_1 and k_2 under all experimental conditions. This material is available free of charge via the Internet at http://pubs.acs.org.

References and Notes

(1) Cline, J. A.; Takahashi, K.; Marin, T. W.; Jonah, C. D.; Bartels, D. M. *J. Phys. Chem. A* **2002**, *106*, 12260−12269.
(2) Janik, I.; Bartels, D. M.; Marin, T. W.; Jonah, C. D. *J. Phys. Chem. A* **2007**, *111*, 79−88.
(3) Lundström, T.; Christensen, H.; Sehested, K. *Radiat. Phys. Chem.* **2002**, *64*, 29−33.
(4) Lundström, T.; Christensen, H.; Sehested, K. *Radiat. Phys. Chem.* **2004**, *69*, 211−216.
(5) Marin, T. W.; Bartels, D. M.; Jonah, C. D. *Chem. Phys. Lett.* **2002**, *371*, 144−149.
(6) Marin, T. W.; Jonah, C. D.; Bartels, D. M. *J. Phys. Chem. A* **2005**, *109*, 1843−1848.
(7) Takahashi, K. J.; Ohgami, S.; Koyama, Y.; Sawamura, S.; Marin, T. W.; Bartels, D. M.; Jonah, C. D. *Chem. Phys. Lett.* **2004**, *383*, 445−450.
(8) Lin, M. Z.; Katsumura, Y.; Muroya, Y.; He, H.; Wu, G. Z.; Han, Z. H.; Miyazaki, T.; Kudo, H. *J. Phys. Chem. A* **2004**, *108*, 8287−8295.
(9) Sims, H. E. *Radiat. Phys. Chem.* **2006**, *75*, 1047−1050.
(10) Christensen, H.; Sehested, K.; Logager, T. *Radiat. Phys. Chem.* **1994**, *43*, 527−531.
(11) Matheson, M. S.; Rabani, J. *J. Phys. Chem.* **1965**, *69*, 1324−1335.
(12) Schwarz, H. A. *J. Phys. Chem.* **1992**, *96*, 8937−8941.

(13) Boyle, J. W.; Ghormley, J. A.; Hochanadel, C. J.; Riley, J. F. *J. Phys. Chem.* **1969**, *73*, 2886−2890.

(14) Brusentseva, S. A. *High Energy Chem.* **1970**, *4*, 339−340.

(15) Buxton, G. V.; Greenstock, C. L.; Helman, W. P.; Ross, A. B. *J. Phys. Chem. Ref. Data* **1988**, *17*, 513−886.

(16) Christensen, H.; Sehested, K. *Radiat. Phys. Chem.* **1980**, *16*, 183−186.

(17) Christensen, H.; Sehested, K. *J. Phys. Chem.* **1986**, *90*, 186−190.

(18) Gordon, S.; Hart, E. J.; Matheson, M. S.; Rabani, J.; Thomas, J. K. *Discuss. Faraday Soc.* **1963**, *36*, 193−205.

(19) Gottschal, W. C.; Hart, E. J. *J. Phys. Chem.* **1967**, *71*, 2102−2106.

(20) Hickel, B.; Sehested, K. *J. Phys. Chem.* **1985**, *89*, 5271−5274.

(21) Meisel, D.; Czapski, G.; Matheson, M. S.; Mulac, W. A. *Int. J. Radiat. Phys. Chem.* **1975**, *7*, 233−241.

(22) Schmidt, K. H.; Bartels, D. M. *Chem. Phys.* **1995**, *190*, 145−152.

(23) Schmidt, K. H.; Hart, E. J. *Adv. Chem. Ser.* **1968**, *81*, 267−279.

(24) Telser, T.; Schindewolf, U. *J. Phys. Chem.* **1986**, *90*, 5378−5382.

(25) Marin, T. W.; Cline, J. A.; Bartels, D. M.; Jonah, C. D.; Takahashi, K. *J. Phys. Chem. A* **2002**, *51*, 12270−12279.

(26) Bartels, D. M.; Takahashi, K.; Cline, J. A.; Marin, T. W.; Jonah, C. D. *J. Phys. Chem. A* **2005**, *109*, 1299−1307.

(27) Cline, J. A.; Jonah, C. D.; Bartels, D. M. *Rev. Sci. Instrum.* **2002**, *73*, 3908−3915.

(28) Wagner, W.; Kruse, A. *Properties of Water and Steam*; Springer-Verlag: Berlin, 1998.

(29) Elliot, A. J. Rate Constants and *G*-Values for the Simulation of the Radiolysis of Light Water over the Range 0−300 °C; report AECL-11073; Chalk River, Ontario, Canada; 1994.

(30) Spinks, J. W. T.; Woods, R. J. *An Introduction to Radiation Chemistry*, 3rd ed.; Wiley-Interscience: New York, 1990.

(31) Pimblott, S. M.; LaVerne, J. A. *J. Phys. Chem. A* **1997**, *101*, 5828−5838.

(32) Pimblott, S. M.; LaVerne, J. A.; Mozumder, A. *J. Phys. Chem.* **1996**, *100*, 8595−8606.

(33) Pimblott, S. M.; LaVerne, J. A. *J. Phys. Chem. A* **2002**, *106*, 9420−9427.

(34) LaVerne, J. A.; Stefanic, I.; Pimblott, S. M. *J. Phys. Chem. A* **2005**, *109*, 9393−9401.

(35) Steinfeld, J. I.; Francisco, J. S.; Hase, W. L. *Chemical Kinetics and Dynamics*; Prentice Hall: Englewood Cliffs, NJ, 1989.

(36) Shiraishi, H.; Sunaryo, G. R.; Ishigure, K. *J. Phys. Chem.* **1994**, *98*, 5164−5173.

(37) Jou, F.-Y.; Freeman, G. R. *J. Phys. Chem.* **1979**, *83*, 2383−2387.

(38) Buxton, G. V.; Elliot, A. J. *J. Chem. Soc., Faraday Trans.* **1993**, *89*, 485−488.

(39) Sehested, K.; Christensen, H. *Radiat. Phys. Chem.* **1990**, *36*, 499−500.

(40) Krynicki, K.; Green, C. D.; Sawyer, D. W. *Faraday Discuss.* **1980**, *66*, 199−208.

(41) Bartels, D. M. *J. Chem. Phys.* **2001**, *115*, 4404−4405.

(42) Schmidt, K. H.; Han, P.; Bartels, D. M. *J. Phys. Chem.* **1992**, *96*, 199−206.

(43) Schmidt, K. H.; Han, P.; Bartels, D. M. *J. Phys. Chem.* **1995**, *99*, 10530−10539.

(44) Kuznetsov, A. M.; Ulstrup, J. *Chem. Phys. Lett.* **1983**, *97*, 285−291.

(45) Sipp, B.; Voltz, R. *J. Chem. Phys.* **1983**, *79*, 434−442.

(46) Barbara, P. F.; Meyer, T. J.; Ratner, M. A. *J. Phys. Chem.* **1996**, *100*, 13148−13168.

(47) Closs, G. L.; Miller, J. R. *Science* **1988**, *240*, 440−446.

(48) Jortner, J. *J. Chem. Phys.* **1976**, *64*, 4860−4867.

(49) Meyer, T. J. *Prog. Inorg. Chem.* **1983**, *30*, 389−440.

(50) Suppan, P. *Top. Curr. Chem.* **1992**, *163*, 95−130.

(51) Brunschwig, B. S.; Sutin, N. *Comments Inorg. Chem.* **1987**, *6*, 209−235.

(52) Harvey, A. H.; Gallagher, J. S.; Levelt Sengers, J. M. H. *J. Phys. Chem. Ref. Data* **1998**, *27*, 761−773.

(53) Roduner, E.; Bartels, D. M. *Ber. Bunsen-Ges. Phys. Chem.* **1992**, *96*, 1037−1042.

(54) Johnson, J. W.; Oelkers, E. H.; Helgeson., H. C. *Comput. Geosci.* **1992**, *18*, 899−947.

(55) Kelly, C. A.; Rosseinsky, D. R. *Phys. Chem. Chem. Phys.* **2001**, *3*, 2086−2090.

(56) Delbuono, G. S.; Rossky, P. J.; Murphrey, T. H. *J. Phys. Chem.* **1992**, *96*, 7761−7769.

(57) Han, P.; Bartels, D. M. *J. Phys. Chem.* **1992**, *96*, 4899−4906.

(58) Hart, E. J.; Anbar, M. *The Hydrated Electron*; Wiley-Interscience: New York, 1970.

(59) Larsen, R. E.; Schwartz, B. J. *J. Phys. Chem. B* **2004**, *108*, 11760−11773.

(60) Larsen, R. E.; Schwartz, B. J. *J. Phys. Chem. B* **2006**, *110*, 9681−9691.

(61) Larsen, R. E.; Schwartz, B. J. *J. Phys. Chem. B* **2006**, *110*, 9692−9697.

(62) Larsen, R. E.; Schwartz, B. J. *J. Phys. Chem. B* **2006**, *110*, 1006−1014.

(63) Schwartz, B. J., personal communication.